

Drag Your Gaussian: Effective Drag-Based Editing with Score Distillation for 3D Gaussian Splatting

Yansong Qu¹, Dian Chen¹, Xinyang Li¹, Xiaofan Li²,

Shengchuan Zhang¹, Liujuan Cao^{1†}, Rongrong Ji¹

¹ Key Laboratory of Multimedia Trusted Perception and Efficient Computing, Ministry of Education of China,
Xiamen University

² Baidu Inc.

{quyans, chendian}@stu.xmu.edu.cn, imlixinyang@gmail.com, shalfunnn@gmail.com
{zsc_2016, caoliujuan, rrj}@xmu.edu.cn

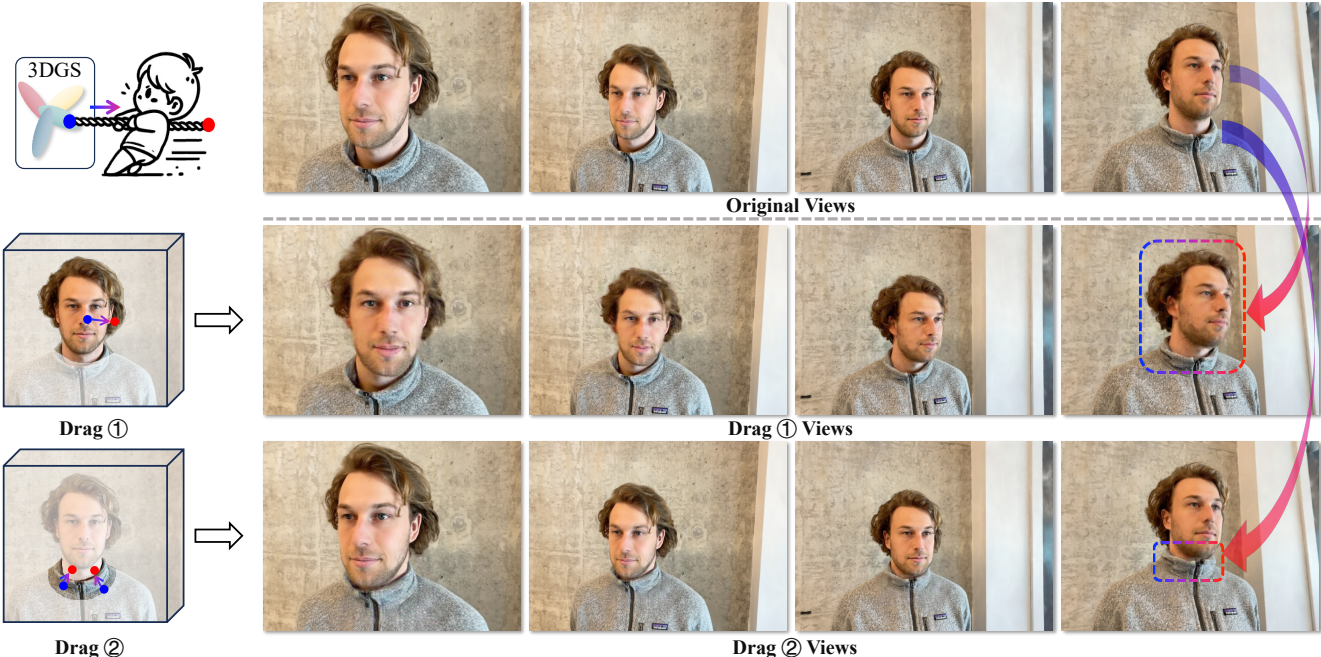


Figure 1: DYG achieves flexible, high-quality drag-based 3D editing results. Given a reconstructed 3D Gaussian field, users specify the desired editing area with 3D masks (brighter areas), and perform scene edits through pairs of control points, including handle points (blue), target points (red).

ABSTRACT

Recent advancements in 3D scene editing have been propelled by the rapid development of generative models. Existing methods typically utilize generative models to perform text-guided editing on 3D representations, such as 3D Gaussian Splatting (3DGS). However, these methods are often limited to texture modifications and fail when addressing geometric changes, such as editing a character's head to turn around. Moreover, such methods lack accurate control over the spatial position of editing results, as language struggles to precisely describe the extent of edits. To overcome these limitations, we introduce DYG, an effective 3D drag-based editing method for 3D Gaussian Splatting. It enables users to conveniently specify the desired editing region and the desired dragging direction through the input of 3D masks and pairs of control points, thereby enabling precise control over the extent of editing. DYG integrates

the strengths of the implicit triplane representation to establish the geometric scaffold of the editing results, effectively overcoming suboptimal editing outcomes caused by the sparsity of 3DGS in the desired editing regions. Additionally, we incorporate a drag-based Latent Diffusion Model into our method through the proposed Drag-SDS loss function, enabling flexible, multi-view consistent, and fine-grained editing. Extensive experiments demonstrate that DYG conducts effective drag-based editing guided by control point prompts, surpassing other baselines in terms of editing effect and quality, both qualitatively and quantitatively. Visit our project page at <https://quyans.github.io/Drag-Your-Gaussian/>.

KEYWORDS

3D Gaussian Splatting, Drag-based Editing, Score Distillation

[†] Corresponding Author.

1 INTRODUCTION

The representation and manipulation of 3D scenes have become increasingly significant in a variety of fields, such as virtual reality (VR) and augmented reality (AR). Traditional 3D representations, such as meshes, voxels, and point clouds, have facilitated many advancements but typically encounter challenges in scalability, efficiency, and expressiveness. The developments in neural scene representations, such as Neural Radiance Fields (NeRF) [19], have suggested impressive capabilities in synthesizing photorealistic novel views. However, NeRF-related methods [4, 21, 28, 35] rely on extensive sampling processes and are computationally intensive, making them less suitable for interactive editing tasks.

Recently, 3D Gaussian Splatting (3DGS) [15] has attracted substantial attention for its ability to represent volumetric data using sparse Gaussian primitives. By replacing dense neural networks with lightweight and interpretable Gaussian primitives, 3DGS enables real-time rendering and fast updates, making it a promising 3D representation for 3D editing. Recent 3DGS-based scene editing methods [5, 6, 34, 37] leverage pre-trained 2D latent diffusion models (LDM) with text prompts to guide the optimization of 3DGS. However, they primarily focus on texture modifications or stylistic changes, falling short in enabling precise geometric editing, as illustrated in Fig. 2.

To overcome these geometric editing limitations, we draw inspiration from recent advancements in 2D drag-based image editing. Methods such as DragGAN [24] and its successors [31, 32] provide precise control and intuitive image editing capabilities through the use of paired control points, including handle points and target points. However, applying 2D drag-based generative models to guide the optimization of 3DGS for drag-based 3D editing introduces a new challenge: the target regions often exhibit sparse distributions of 3D Gaussians, making it challenging to effectively edit the 3D Gaussian field. Consequently, the model tends to align the texture of nearby 3D Gaussians around the target area, rather than accurately generating the desired geometric structures. This issue significantly impacts the precision and realism of the editing results.

A straightforward approach involves adopting a rigid transformation [35, 38], where 3DGS primitives around the handle points are copied to the target region during initialization. However, it significantly limits the diversity of editing tasks and often results in poor geometry in the target area, leading to noticeable artifacts.

In this work, we present **Drag Your 3D Gaussian** (DYG), a novel drag-based 3DGS editing approach for real-world scenes. To enhance usability and accessibility, we extend the 2D drag-based image editing paradigm to 3D, introducing 3D masks along with pairs of 3D control points as inputs for editing 3D scenes. We integrate the independence and discreteness of 3DGS with the continuous nature of implicit triplane representation to address the challenge of sparse 3D Gaussian distributions. To encode the positions of 3D Gaussians, we introduce the Multi-scale Triplane Positional (MTP) Encoder, and employ a Region-Specific Positional (RSP) Decoder to predict positional offsets, constructing the geometric scaffold for dragging. Additionally, we propose a Soft Local Edit (SLE) strategy to focus editing on the desired region while preserving the integrity of other areas. Leveraging an off-the-shelf 2D drag-based

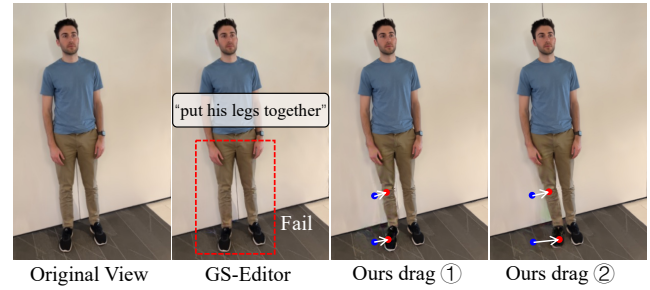


Figure 2: Differences between our drag-based editing approach and the text-guided editing method GS-Editor [6]. The latter often fails to achieve geometric editing goals and struggles to describe the degree of editing through text, whereas our method allows for flexible control over the extent of edits.

LDM as supervision through the proposed Drag-SDS loss function, we enable perceptually plausible scene dragging with multi-view consistency. As shown in Fig. 1 and Fig. 2, DYG facilitates flexible and fine-grained 3D scene editing.

Our contributions can be summarized as follows:

- We propose an effective drag-based scene editing method for 3D Gaussian Splatting, capable of delivering flexible and high-quality results for geometric editing tasks, including deformation, transformation, and morphing.
- We introduce the MTP encoder to address the challenge of uneven spatial distribution of Gaussian primitives, facilitating smooth geometric editing. Additionally, the RSP decoder and SLE strategy ensure harmonious local editing. Finally, Drag-SDS leverages the existing 2D drag-based LDM to achieve multi-view consistent dragging results.
- Extensive experiments quantitatively and qualitatively demonstrate that our method achieves state-of-the-art (SOTA) 3D scene editing results, validating the versatility and generalization capabilities of DYG.

2 RELATED WORK

2.1 Drag-based Image Editing

In light of advancements in generative models, image editing has seen significant development. However, text-guided image editing methods [2, 10, 14, 29] often lack precision and flexibility when it comes to editing spatial attributes. To address this, DragGAN [24] enables impressive interactive drag-based image editing by utilizing control points and optimizing generative adversarial networks (GANs) latent codes. However, the applicability of this framework is constrained by the intrinsic limitations in the capacity of GANs. In order to enhance generalization, subsequent works [18, 20, 32] extend this paradigm to large-scale Latent Diffusion Models (LDM). However, these methods depend on computationally intensive operations, such as latent optimization, resulting in inefficiencies in editing tasks.

Lightning-Drag [31] encodes user prompts into corresponding point embeddings, which are then injected into the self-attention

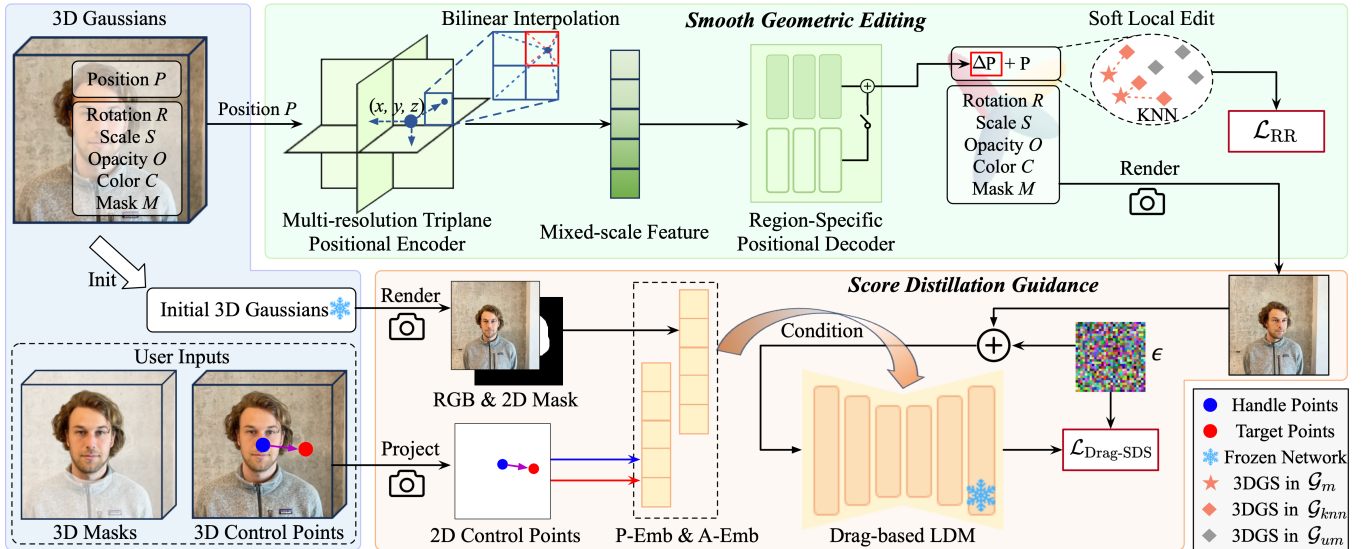


Figure 3: The overall framework of DYG. Left: Given a 3D Gaussian scene, users provide 3D masks and several pairs of control points as input. Top-right: The Smooth Geometric Editing module predicts positional offsets for 3D Gaussians, resolving the issue of sparse distributions within the target region while ensuring seamless local editing. We adopt a two-stage training strategy: the first stage constructs the geometric scaffold of the edited Gaussians, and the second stage refines the texture details. Bottom-right: In the Score Distillation Guidance Module, to ensure stable optimization, 3D control points are projected onto 2D control points for a specified viewpoint. The RGB image and 2D mask, rendered from the mirrored initial 3D Gaussians, are encoded into point embeddings (P-Emb) and appearance embeddings (A-Emb), which act as conditions for the drag-based LDM. This process leverages our proposed Drag-SDS loss function to enable flexible and view-consistent 3D drag-based editing.

modules of the Stable Diffusion inpainting backbone [11, 33] to guide the generation process. This approach eliminates the need for time-consuming operations required in previous methods [22, 32], enabling interactive drag-based image editing. In this work, we adopt Lightning-Drag [31] as the guiding model for editing 3DGS, owing to its rapid and high-quality drag-based editing capabilities.

2.2 3D Editing for Radiance Fields

Neural Radiance Fields (NeRF) [19] introduced radiance fields, having excelled in novel view synthesis, producing realistic rendering results. However, NeRF’s reliance on a neural network for complete implicit representation of scenes leads to tedious training and rendering times. More recently, 3DGS [9] has garnered attention from researchers due to its real-time rendering speed and photo-realistic rendering quality.

Robust 3D representations have driven advancements in 3D editing. Early methods [8, 23, 40] learn object-compositional NeRFs, enabling object-level editing, such as duplicating or moving objects. However, these approaches are limited to coarse-grained manipulations. Works like NeuMesh [39] and related methods [35, 38, 42] propose using explicit geometry, such as cages or point clouds, to facilitate geometric editing. Nevertheless, these methods heavily rely on precise geometric reconstructions. SC-GS [13] adopts a sampling-based approach to learn anchor points for editing 3D scenes. However, these methods strongly depend on accurate geometric representations, offer limited editing diversity, and often suffer from unreasonable results, such as local tearing artifacts.

With the success of generative models, methods [9, 34, 44, 45], like GS-Editor [6] and GS-Ctrl [37] leverage text-guided latent diffusion models for 3D scene editing. While effective for texture or style modifications, these approaches often fail to handle geometric changes. Moreover, they struggle to accurately specify the spatial extent of editing through text. In contrast, our method enables flexible, fine-grained geometric editing while maintaining the plausibility of the edited scenes.

3 PRELIMINARY

3.1 3D Gaussian Splatting

3D Gaussian Splatting (3DGS) [15] utilizes a set of anisotropic 3D Gaussians to model three-dimensional information and provide fast rendering by efficiently rasterizing 3D Gaussians into images, given camera poses. Specifically, each Gaussian is composed of its position $p \in \mathbb{R}^3$, a scale $s \in \mathbb{R}^3$, a rotation quaternion $r \in \mathbb{R}^4$, an opacity $o \in \mathbb{R}$, and the spherical harmonics (SH) coefficients $c \in \mathbb{R}^d$ for volume rendering. These 3D Gaussians are projected onto the image plane as 2D Gaussians and rendered in real time using the tiled rasterizer.

3.2 Score Distillation Sampling (SDS)

DreamFusion [26] introduces the SDS loss function, utilizing a pre-trained 2D latent diffusion model (LDM) to optimize 3D representations for 3D generation. Specifically, given a differentiable 3D representation, such as NeRF [19] or 3DGS [15], parameterized by

\mathcal{G} and a rendering function \mathcal{R} , the rendered image corresponding to a camera pose c can be expressed as $x = \mathcal{R}(\mathcal{G}, c)$. SDS leverages the prior knowledge of a LDM to guide the optimization of the 3D representation \mathcal{G} in a low-resolution latent space. This latent space is articulated as $z = \mathcal{E}(x)$, $x = \mathcal{D}(z)$, where \mathcal{E} and \mathcal{D} represent the encoder and decoder of the LDM, respectively. The SDS loss function is formulated as follows:

$$\nabla_{\mathcal{G}} \mathcal{L}_{\text{SDS}} = \mathbb{E}_{t, \epsilon, c} \left[w(t) (\hat{\epsilon} - \epsilon) \frac{\partial \mathcal{E}(\mathcal{R}(\mathcal{G}, c))}{\partial \mathcal{G}} \right] \quad (1)$$

where ϵ denotes ground truth noise, $\hat{\epsilon}$ is the noise predicted by the LDM with z_t as input for timestep t , and $w(t)$ represents a weighting function that varies according to the timestep t . The SDS loss can be reformulated [33, 43] as follows:

$$\mathcal{L}_{\text{SDS}} = \mathbb{E}_{t, \epsilon, c} \left[w(t) \frac{\sqrt{\bar{\alpha}_t}}{\sqrt{1 - \bar{\alpha}_t}} \|z - \hat{z}\|_2^2 \right], \quad (2)$$

where

$$\hat{z} = \frac{z_t - \sqrt{1 - \bar{\alpha}_t} \hat{\epsilon}}{\sqrt{\bar{\alpha}_t}}, \quad (3)$$

with $\bar{\alpha}(t)$ is also a weighting function that dynamically varies with each timestep t .

4 METHODS

4.1 Problem Definition and Method Overview

Given a reconstructed 3D Gaussian field \mathcal{G} , we extend the attributes of 3D Gaussians by adding a mask attribute m , which represents the user-defined 3D masks for the desired editing area. The Gaussian field \mathcal{G} can be defined as: $\mathcal{G} = \{p_i, r_i, s_i, \alpha_i, c_i, m_i\}_{i=1}^N$. In addition to the 3D mask, users are also required to input K pairs of control points $Q = \{(q_i^o, q_i^t)\}_{i=1}^K$, where $q_i^o, q_i^t \in \mathbb{R}^3$ serve as guidance for the editing process. Our objective is to drag the the desired editing region around the handle points q_i^o to the target points q_i^t .

Rendering and Projection for 2D Guidance. In order to ensure stable control of the 2D drag-based LDM, a mirrored copy of \mathcal{G} is preserved, referred to as the Initial 3D Gaussians \mathcal{G}' , as shown in Fig. 3. During the training phase, for a given camera pose c , an RGB image I_c and a 2D mask are rendered from \mathcal{G}' using the similar volumetric rendering approach [15, 27]. This 2D mask is then subjected to a dilation operation to produce the final 2D mask M_c . Additionally, the 3D control points Q are projected into 2D points $Q_c^{2d} = \{(\Pi(q_i^o), \Pi(q_i^t))\}_{i=1}^K$, through the projection transformation Π . Upon acquiring I_c , M_c and view-specific 2D control points Q_c^{2d} obtained, these inputs are utilized as the condition y of 2D drag-based LDM to guide 3DGS optimization using our proposed Drag-SDS loss.

Local Edit. Our guiding principle is to perform localized edits within the desired editing region while ensuring that the rest of the scene remains unaffected, thereby maintaining overall harmony and realism.

To facilitate this process, we have developed an interactive GUI tool based on 3D Gaussian Splatting. This tool enables users to identify desired editing regions from different viewpoints and generates the 3D mask by calculating the intersection of 3D Gaussians within each view frustum. This real-time interactive approach allows users to efficiently complete the 3D mask selection process with minimal effort, potentially requiring only a single operation.

Method Overview. Figure 3 illustrates the overview of our method. In Sec. 4.2, we explain how to integrate the strengths of the implicit triplane representation and explicit 3DGS to overcome suboptimal editing outcomes caused by the sparsity of 3DGS in target regions, thereby enabling high-quality, localized drag-based editing. In Sec. 4.3, we describe how the existing 2D drag-based LDM is incorporated into our method through the proposed Drag-SDS loss function, enabling flexible, view-consistent, and fine-grained editing.

4.2 Smooth Geometric Editing

3D drag-based editing encompasses three main scenarios: (1) Deformation: Involves fine-grained edits, such as adjusting facial features to face a different direction. (2) Transformation: Encompasses local rigid transformations, exemplified by moving a man’s leg to take a step forward. (3) Morphing: Includes structural adjustments, such as to raise the collar or to make a person’s shoulders narrower.

For scenario (1), the challenge lies in fine-grained local editing—modifying the desired region while preserving other areas as much as possible. For scenarios (2) and (3), the key challenge lies in the sparsity of 3D Gaussians around the target points, making it difficult to generate new Gaussians within the target region through optimization or the densify and prune operations [15]. This often results in editing failures.

Therefore, based on the above observations and to propose a unified solution, we present the Multi-resolution Triplane Positional Encoder, Region-Specific Positional Decoder, Two-stage Dragging, and Soft Local Editing strategies to achieve smooth geometric editing.

Multi-resolution Triplane Positional (MTP) Encoder. The triplane representation [3, 7, 46] is distinguished by its compactness and efficient expressiveness. Its implicit nature facilitating the learning of 3D structures through volume rendering [15, 28], providing an effective solution to the uneven spatial distribution of Gaussian primitives.

Another consideration is that the intuitive approach for 3D drag-based editing should involve moving the original region’s Gaussians primitives to the target region, rather than deleting the primitives in the original region and generating new ones in the target region. To achieve this, we introduce the Multi-resolution Triplane Positional (MTP) Encoder to encode the position of the 3D Gaussians and predict the position shifts ΔP with the Region-Specific Positional Decoder.

Specifically, the MTP decomposes the 3D space into three orthogonal, learnable multi-resolution feature planes: \mathcal{H}_{xy} , \mathcal{H}_{xz} , \mathcal{H}_{yz} . For the position $p = (x, y, z)$ of each 3D Gaussian, it is normalized and projected onto these triplanes at varying resolutions:

$$f_c^s = \psi^s(\mathcal{H}_c, \pi_c(x, y, z)), \quad (4)$$

$$f = \Theta(\text{concat} \prod_{c \in C} f_c^s), \quad (5)$$

where π_c projects the point onto the c -th plane, and ψ^s performs bilinear interpolation on the plane at resolution s . \prod denotes the Hadamard product, C represents the set of planes $\{xy, xz, yz\}$, and Θ is a lightweight MLP for fusing positional mixed-scale features.

Region-Specific Positional (RSP) Decoder. We introduce the local editing guiding principle in Sec. 4.1, however, the implicit

representation of triplane, combined with the latent-based optimization of SDS, inevitably result in changes to regions outside the 3D mask. To address this issue, the RSP decoder predict the position shifts Δp of the masked 3DGS while introducing a new network to correct the unintended movements in regions outside the 3D masks. Additionally, we propose a regularization loss to further constrain the optimization process. Specifically, The 3DGS \mathcal{G} is divided into two subsets: $\mathcal{G}_m = \{(p_i, r_i, s_i, o_i, c_i, m_i) \in \mathcal{G} \mid m_i = 1\}$ and $\mathcal{G}_{um} = \{(p_i, r_i, s_i, o_i, c_i, m_i) \in \mathcal{G} \mid m_i = 0\}$. two MLPs, \mathcal{N}_1 and \mathcal{N}_2 , are employed as decoders for the feature f obtained from the MTP encoder. The position shift of each Gaussian primitive g_i can be formulated as follows:

$$\Delta p = \begin{cases} \mathcal{N}_1(f) & \text{for } g_i \in \mathcal{G}_m \\ \text{sg}(\mathcal{N}_1(f)) + \mathcal{N}_2(\text{sg}(f)) & \text{for } g_i \in \mathcal{G}_{um}, \end{cases} \quad (6)$$

where $\text{sg}(\cdot)$ is the stop gradient operator. Based on this, we design a region regularization loss to encourage the unmasked Gaussians to remain unchanged:

$$\mathcal{L}_{RR} = \sum_{g_i \in \mathcal{G}_{um}} \Delta p_i. \quad (7)$$

Two-stage Dragging. The entire dragging process consists of two stages. The first stage focuses on optimizing the geometric structure, thereby establishing the foundational geometric scaffold of the edited scene. During this stage, the model optimizes both the MTP encoder and RSP decoder while freezing all 3DGS parameters and halting the densify and prune operations [15]. As shown in Fig. 10 In the complex deformation task of turning a character’s face, after Stage 1, the Gaussians corresponding to the face are dragged to the target region, while the positions of unmasked Gaussians remain unchanged. The second stage focuses on refining the texture details of the scene. During this stage, other attributes of the 3D Gaussians (color, opacity, rotation, and scale) are primarily optimized, and the densify and prune operations are reactivated. After constructing the basic geometric scaffold in the first stage, the regions outside the desired editing area tend to remain unchanged during the second stage. The newly added 3D Gaussians primarily originate from the splitting or duplication of elements in \mathcal{G}_m . Consequently, all newly added 3D Gaussians are assigned to \mathcal{G}_m for subsequent optimization.

Soft Local Edit (SLE). Strictly freezing the parameters of 3DGS outside the 3D mask [6, 34] to facilitate local editing may result in disjoint effects, as illustrated in Fig. 7(e). To address this limitation, we adopt a soft 3D mask strategy. Specifically, for each 3D Gaussian within \mathcal{G}_m , we identify its K-nearest neighbors (KNN) and select those belonging to \mathcal{G}_{um} to form the set \mathcal{G}_{knn} . These neighboring Gaussians are subsequently optimized with a reduced learning rate to ensure smoother transitions.

4.3 Score Distillation Guidance

The SDS loss [26], which leverages LDM as the guidance model to produce multi-view consistent 3D results, has been widely adopted in 3D generation methods [17, 36, 45]. However, it suffers from issues of over-saturation, over-smoothing. Inspired by [16, 41], we extend SDS and propose an improved score distillation loss function. For the predicted noise $\hat{\epsilon}$ in Eq. (1), we extend it into a composite

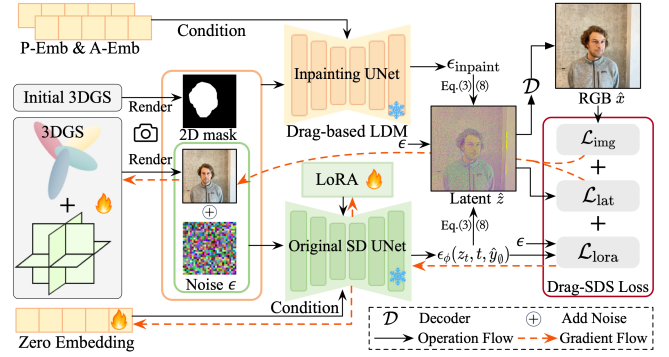


Figure 4: Detailed illustration of Score Distillation Guidance Module and Drag-SDS loss, presented in Fig. 3. We employ two different UNets to predict ϵ_{tgt} and ϵ_{src} described in Eq. (8), respectively. The components within the orange box represent the inputs to the Inpainting UNet, while the components within the green box signify the inputs to the Original SD UNet.

term defined as follows:

$$\hat{\epsilon} = \epsilon_{tgt} - \epsilon_{src} + \epsilon, \quad (8)$$

where ϵ_{tgt} represents the noise predicted by the LDM, ϵ_{src} denotes a learnable source prediction for adaptive estimation of the current distribution.

Our guidance model, Lightning-Drag [31], employs the Stable Diffusion Inpainting U-Net as the backbone to predict ϵ_{tgt} . It takes as input the concatenation of noise latents z_t , a binary mask m_{2d} , and the latents of the masked initial image $m_{2d} \odot x_0$. The model also incorporates the point embedding of 2D control points and the appearance embedding as the condition y . For clarity, we omit the classifier-free guidance [26, 41]. As shown in Fig. 4, the output of our guidance model is represented as $\hat{\epsilon}_{inpaint} = \epsilon_{\theta}(z_t, t, y, m_{2d}, \mathcal{E}(m_{2d} \odot x_0))$. Our Drag-SDS loss is composed of three components: image-space loss \mathcal{L}_{img} , latent-space loss \mathcal{L}_{lat} , and \mathcal{L}_{lora} .

Lightning-Drag provides reliable predictions for ϵ_{tgt} ; however, it is not suitable for estimating ϵ_{src} . This limitation stems from the inpainting backbone tends to focus primarily on the information within the masked region while preserving the content outside the mask, thereby failing to fully capture the current distribution. Therefore, different from straightforwardly using the same UNet to predict ϵ_{tgt} and ϵ_{src} in [16, 41], we utilize the original Stable Diffusion UNet with a LoRA model [12] ϕ as the predictor of ϵ_{src} , denoted as $\hat{\epsilon}_{\phi}(x_t, t, \hat{y}_0)$, where \hat{y}_0 is a learnable embedding initialized to zero. The LoRA model is trained using a simple diffusion loss, defined as:

$$\mathcal{L}_{lora} = \mathbb{E}_{t,c,\epsilon} [\|\epsilon_{\phi}(x_t, t, \hat{y}_0) - \epsilon\|_2^2] \quad (9)$$

The latent-space score objective, referred to as \mathcal{L}_{lat} , is formulated similarly to Eq. (2). The image-space score distillation loss function is defined as follows:

$$\mathcal{L}_{img} = \mathbb{E}_{t,c,\epsilon} \left[w(t) \frac{\sqrt{\bar{\alpha}_t}}{\sqrt{1 - \bar{\alpha}_t}} \|x - \hat{x}\|_2^2 \right], \quad (10)$$

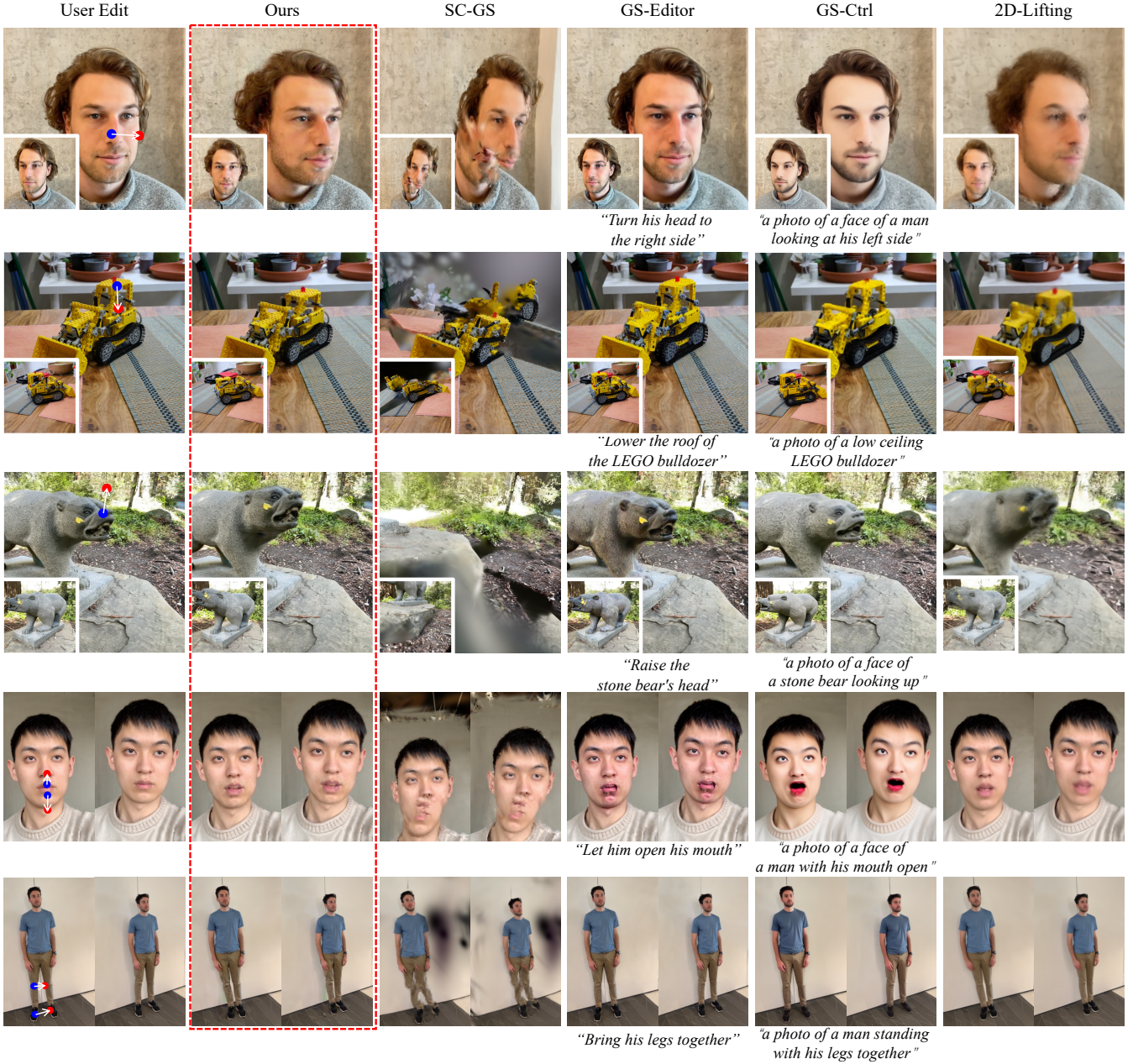


Figure 5: Qualitative comparison between DYG and different baselines. The first column shows two rendered views of the original 3D scene, where the 3D editing points are projected onto the 2D plane for visualization. SC-GS [13] often results in scene-tearing artifacts, while GS-Editor [6] and GS-Ctrl [37] frequently fail to perform successful edits. Additionally, GS-Ctrl tends to exhibit over-saturation issues, and 2D-Lifting suffers from scene blurriness. By contrast, our approach is able to sufficiently interpret both the user's dragging intent and the 3D scene context, thereby achieving effective editing and generating high-quality, detailed results across various scenarios, including deformation, transformation, morphing.

where $\hat{x} = \mathcal{D}(\hat{z})$, with \mathcal{D} is the image decoder of LDM. The final Drag-SDS loss function can be defined as:

$$\mathcal{L}_{\text{Drag-SDS}} = \lambda_{\text{lat}} \mathcal{L}_{\text{lat}} + \lambda_{\text{img}} \mathcal{L}_{\text{img}} + \lambda_{\text{lora}} \mathcal{L}_{\text{lora}}, \quad (11)$$

where λ_{lat} , λ_{img} , λ_{lora} represent the weights for the latent-space, image-space, and lora objectives, respectively.

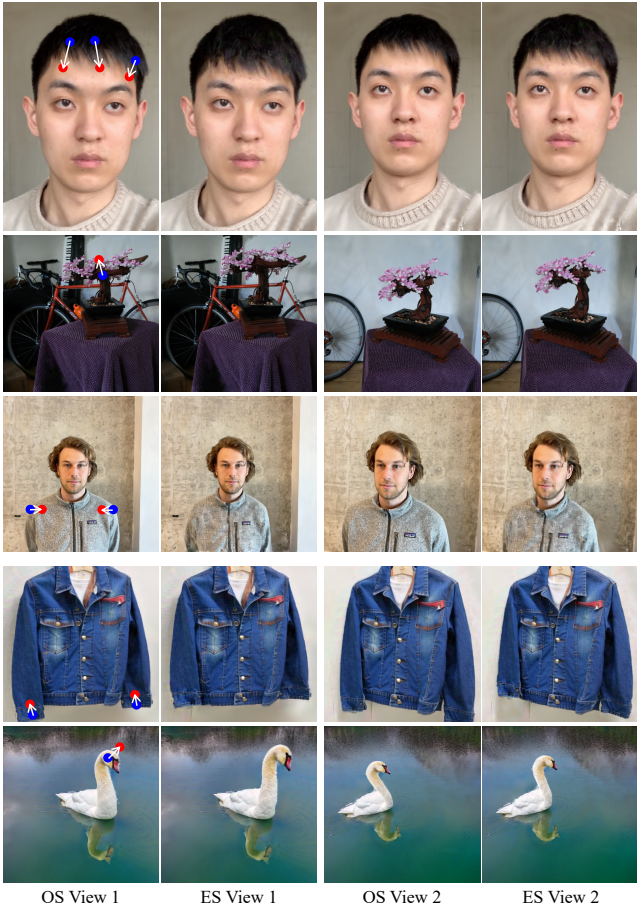


Figure 6: More qualitative results. The top three rows showcase real scenes, while the bottom two rows are generated scenes. For each edit, we show two views of both the original (OS) and edited scenes (ES).

5 IMPLEMENTATION DETAILS

Our model, built on a 3D Gaussian Scene reconstructed using vanilla 3D Gaussian Splatting [15], completes one dragging operation on an A100-40G GPU in approximately 10 minutes, whereas GS-Editor [6] requires over 20 minutes.

Additional implementation details are provided in the Appendix.

6 EXPERIMENTS

6.1 Evaluation Setup

Baseline Methods. It should be noted that this is the first work to perform 3DGS drag-based editing in real scenes, and therefore there are no directly comparable baselines. We compare our method with other 3DGS-based text-driven editing approaches, including GS-Editor [6] and GS-Ctrl [37], as well as the anchor point-based dragging method SC-GS [13]. Additionally, we construct a naive baseline, 2D-Lifting, which uses the same inputs as our method but performs drag-based editing on 2D images with our guidance model, Lightning-Drag [31], followed by 3D reconstruction [15].

Datasets. To comprehensively evaluate our method, we select six representative scenes from two datasets: Mip-NeRF360 [1] and Instruct-NeRF2NeRF [9]. We perform over 20 types of editing tasks on these scenes, which include human faces, indoor objects, and complex outdoor scenes.

6.2 Qualitative Evaluation

Since no other existing methods currently support 3D drag-based editing for real scenes, we make our best effort to guide SC-GS, GS-Editor, and GS-Ctrl to achieve comparable editing results, ensuring a fair comparison.

Fig. 5 presents the results of our method compared to other approaches. The editing results illustrate that our approach enables flexible edits while ensuring high visual quality and multi-view consistency. For instance, in the first row, we demonstrate a deformation scenario: dragging the face to one side, which is a highly challenging task. This is because the operation not only involves rotating the entire head but also requires the facial features, such as the eyes, to change harmoniously and synchronously to maintain consistency and realism. It can be observed that SC-GS exhibits tearing artifacts in the scene, while GS-Editor only shows minor darkening in color without effective geometric changes. GS-Ctrl achieves slightly more noticeable changes, but similar to GS-Editor, it fails to perform meaningful geometric editing. 2D-Lifting manages to turn the head, but severe inconsistencies across views result in significant scene blurriness. By contrast, our method successfully turns the head to one side while maintaining better details.

Fig. 6 showcases more results on additional scenes, demonstrating its ability to handle complex scenarios. These results illustrate that our method effectively interprets the control-point prompts and produces plausible, high-quality 3D drag-based edits.

6.3 Quantitative Evaluation

As there is currently no widely accepted benchmark dataset for 3D scene editing, we conducted user studies to evaluate the editing results and quality. To ensure objectivity, we also adopted the GPT Evaluation Score as an additional metric. Furthermore, we utilized aesthetic evaluation metrics [30] to assess the quality of the edited scenes.

User Study. We collected survey responses from 75 users, with each questionnaire containing comparisons of 10 edited scenes. Users were asked to select their preferred editing results based on two criteria: Edit Effect and Scene Quality, respectively, resulting in a total of 1,500 votes. Fig. 9 visualizes the results of the user study, showing that 86.1% and 62% of users favored our editing results, significantly outperforming other compared methods.

GPT Score. We utilized GPT-4o to evaluate the editing results of different methods, asking it to rate the results based on three criteria: Scene Quality (SQ), which assesses the visual quality of the edited scene; Editing Effect (EE), which examines whether the editing result meets the intended requirements; and Retention of Initial Features (RIF), which evaluates whether non-edited regions remain unchanged. Scores were assigned on a scale from 0 to 5 for each criterion. Table 1 presents the average scores across all editing scenarios, with the GPT-Overall (GPTO) score calculated as $0.3 \times \text{SQ} + 0.4 \times \text{EE} + 0.3 \times \text{RIF}$. The first row shows the scores

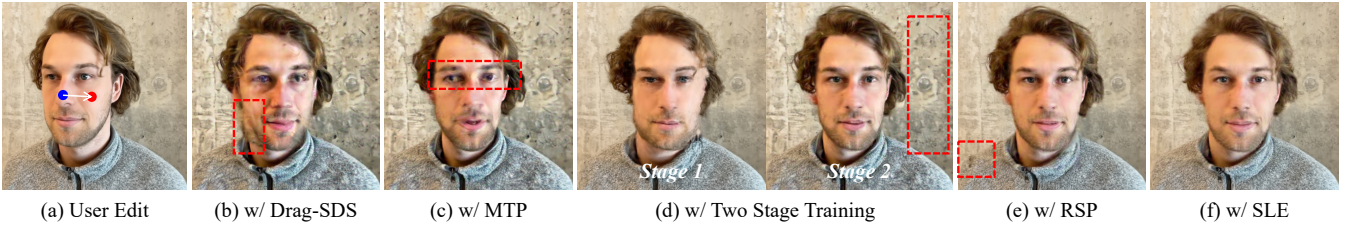


Figure 7: Ablation Study on different modules of DYG. From left to right, new modules are progressively added on top of the previous setup.

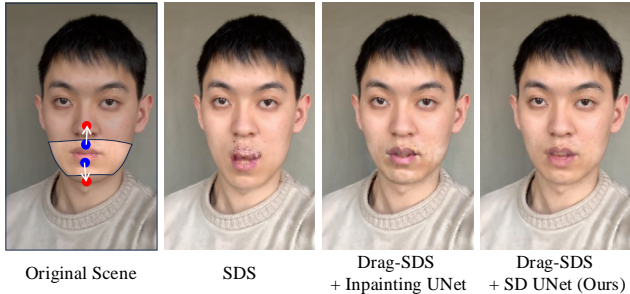


Figure 8: Ablation Study of different score distillation loss functions. To visualize the 3D mask, we render it as a 2D mask, with the bright region indicating masked area and the darker region unmasked. SDS [26] often causes blurriness in the desired editing area, while Drag-SDS with the inpainting UNet over-focuses on the mask, creating disharmonious color layers. By contrast, our method delivers harmonious editing results.

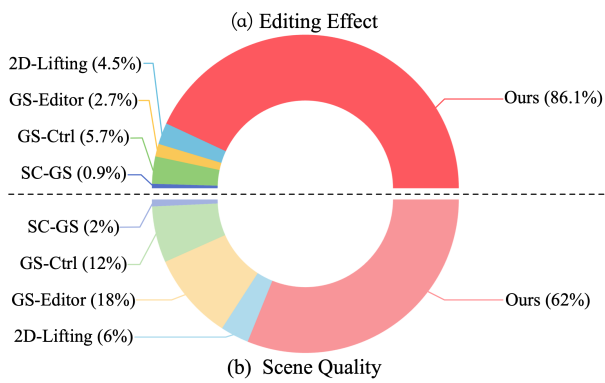


Figure 9: User study of different methods for 3D scene editing.

for the initial, unedited scenes, which receive a rating of 5 in all categories.

Analyzing in conjunction with Fig. 5 and Table 1, SC-GS receives low scores due to extensive tearing artifacts. GS-Editor achieves a relatively high RIF score because of minimal geometric changes but has a low EE score as the edits are less effective. GS-Ctrl often fails in geometric editing, resulting in a low EE score. 2D-Lifting,

Table 1: Evaluation metrics. We report the Scene Quality (SQ), Editing Effect (EE), Retention of Initial Features (RIF), GPT-Overall (GPTO), and Aesthetic (AES) scores for different methods across various scenes. Gray text represents the evaluation metrics of the initial scene.

	SQ↑	EE↑	RIF↑	GPTO↑	AES↑
Init	5		5		5.53
SC-GS [13]	2.69	2.318	2.28	2.4182	4.14
GS-Editor [6]	4.418	2.354	4.624	3.6542	5.28
GS-Ctrl [37]	4.162	2.16	4.392	3.4302	5.38
2D-Lifting	3.116	3.234	3.212	3.192	4.85
Ours	4.434	4.42	4.626	4.486	5.36

which reconstructs scenes after 2D dragging, generally succeeds in geometric edits but suffers from multi-view inconsistencies, leading to blurry results and consequently low SQ scores. By contrast, our method achieves the best performance across all four metrics.

Aesthetic Score. We evaluate the aesthetic quality of 3D edit results using the open-source LAION Aesthetics Predictor, which rates image quality on a 0–10 scale. The rendered images of edited 3D scenes are scored, and the average is reported. As shown in the last column of Table 1, our method decreases by only 0.17 compared to the initial score, achieving better performance compared to SC-GS [13], GS-Editor [6], and 2D-Lifting. Notably, GS-Ctrl tends to oversaturate the overall scene colors, leading to higher aesthetic scores. For example, in the first column of Fig. 5, The face becomes smoother and more cartoon-like, resulting in a higher aesthetic score, but it fails to achieve the intended head-turning editing operation.

6.4 Ablation Study

Smooth Geometric Editing module. To evaluate the effectiveness of the design of our Smooth Geometric Editing module, we conduct an ablation study and can be shown in Fig. 7. From left to right, we progressively add new modules on top of the previous setup. Fig. 7(b): Only the Drag-SDS loss function is used to guide optimization, with all 3DGS parameters trainable. The results show a tendency to fit the target distribution through texture adjustments rather than position shifts, leaving artifacts where original Gaussians fail to move completely to the target region, such as the lower left corner of the face. Fig. 7(c): Introducing MTP with other Gaussian parameters trainable. While this alleviates

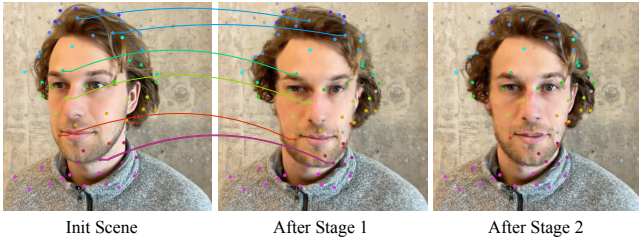


Figure 10: Visualization of the positional changes of sampled 3D Gaussians after two-stage dragging. The positions of masked 3D Gaussians are represented as colored points, while others are shown in gray.

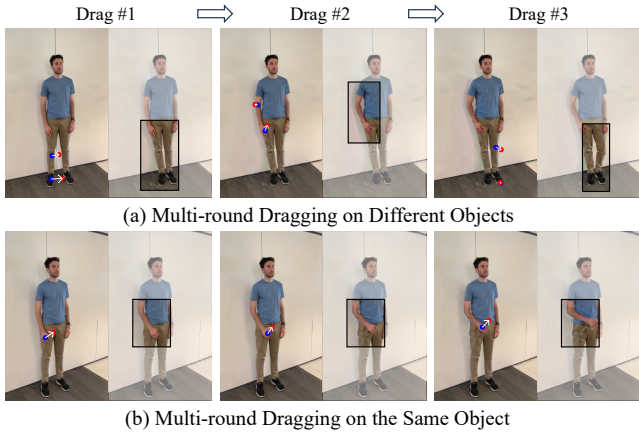


Figure 11: Multi-round Dragging. Each dragging operation is performed based on the results of the previous edit shown on the left.

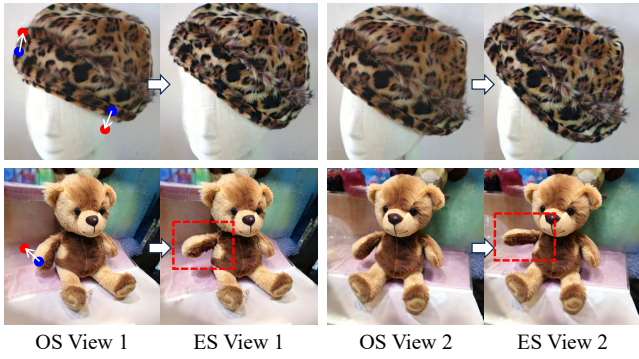


Figure 12: Visualization of dragging on the generated scenes. For each edit, we show two views of both the original (OS) and edited scenes (ES).

the Gaussian artifact issue, the fine-grained dragging performance remains unsatisfactory. Fig. 7(d): A two-stage optimization strategy is introduced. In the first stage, only MTPE and RPD are optimized, aligning the target distribution via Gaussian displacements to build

a scaffold for the edited scene. In the second stage, Gaussian parameters are learned to refine the scene representation. However, this approach unintentionally modifies the background, leading to issues like over-saturation and darkened colors. Fig. 7(e): Local Edit is applied, but it introduces cracks between the 3D mask region and surrounding areas, such as the region around the shoulders. Fig. 7(f): Finally, the Soft Local Edit strategy is introduced, achieving the highest visual quality with harmonious and consistent results.

Effectiveness of Drag-SDS. We conduct an ablation study on different distillation loss functions. All training strategies and modules are identical to the full model, with the only difference being the choice of the distillation loss function. As shown in Fig. 8, SDS [26] results in a blurred target region, failing to achieve the desired action, such as opening the mouth. In contrast, our proposed Drag-SDS method successfully enables target editing. However, due to its reliance on an inpainting strategy, it focuses more on estimating the image distribution within the mask, leading to inconsistent colors between masked and unmasked regions. For example, the area around the mouth appears lighter, causing noticeable layering artifacts. In comparison, our approach, which utilizes the original SD [11, 33] UNet, pays greater attention to global information and effectively resolves this issue.

6.5 Multi-round Dragging

Due to the complexity and diversity of editing tasks, there arises a demand for multi-round dragging. As shown in Fig. 11, we explore the potential of extending DYG to multi-round dragging scenarios. In Fig. 11(a), we perform sequential edits on different targets (e.g., right leg, right arm, left leg), building upon the results of the previous round. Similarly, Fig. 11(b) shows multi-round editing applied to the same target (e.g., gradually raising the man's right arm). The results illustrate that DYG can be easily adapted to multi-round dragging scenarios while maintaining notable stability.

6.6 Dragging for 3D Generative Scenes

In addition to real-world scenes, we also explore the application of our method to editing 3D generative scenes. As shown in Fig. 12, we leverage Director3D [16] to generate two scenes with the text prompts “A faux-fur leopard print hat” and “A brown teddy bear in a toy shop,” respectively. Subsequently, we apply drag-based editing to these scenes. To our delight, our DYG presents strong generalization to 3D generative results, achieving high-quality and precise drag-based editing even in these synthetic scenarios. More examples of scene edits in generated scenarios can be found in the last two rows of Fig. 6.

7 LIMITATION AND CONCLUSION

Limitation. Our method distills prior knowledge from 2D drag-based LDM to optimize the 3D Gaussian primitives. Although DYG satisfies a diverse range of 3D drag-based editing requirements, our 3D editing capabilities are inherently limited by the performance of 2D generative models. Therefore, advancements in 2D generative models can further drive the development of our method.

Conclusion. We present DYG, an effective drag-based scene editing method that enables users to conveniently perform flexible, fine-grained, high-quality edits on 3D Gaussian scenes using 3D

masks and control points. Extensive experiments demonstrate the effectiveness and generalization of our method. Our future work includes improving interaction speed to achieve near-real-time 3D drag-based editing. Additionally, it can be extended to 4D dynamic processes, enabling dynamic editing results for 3D scenes.

REFERENCES

[1] Jonathan T. Barron, Ben Mildenhall, Dor Verbin, Pratul P. Srinivasan, and Peter Hedman. 2022. Mip-NeRF 360: Unbounded Anti-Aliased Neural Radiance Fields. In *IEEE/CVF Conference on Computer Vision and Pattern Recognition, CVPR 2022, New Orleans, LA, USA, June 18–24, 2022*. IEEE, 5460–5469. <https://doi.org/10.1109/CVPR52688.2022.00539>

[2] Tim Brooks, Aleksander Holynski, and Alexei A Efros. 2023. Instructpix2pix: Learning to follow image editing instructions. In *Proceedings of the IEEE/CVF Conference on Computer Vision and Pattern Recognition*. 18392–18402.

[3] Eric R Chan, Connor Z Lin, Matthew A Chan, Koki Nagano, Boxiao Pan, Shalini De Mello, Orazio Gallo, Leonidas J Guibas, Jonathan Tremblay, Sameh Kamhis, et al. 2022. Efficient geometry-aware 3d generative adversarial networks. In *Proceedings of the IEEE/CVF conference on computer vision and pattern recognition*. 16123–16133.

[4] Anpei Chen, Zexiang Xu, Andreas Geiger, Jingyi Yu, and Hao Su. 2022. Tensorf: Tensorial radiance fields. In *European conference on computer vision*. Springer, 333–350.

[5] Minghao Chen, Iro Laina, and Andrea Vedaldi. 2025. Dge: Direct gaussian 3d editing by consistent multi-view editing. In *European Conference on Computer Vision*. Springer, 74–92.

[6] Yiwen Chen, Zilong Chen, Chi Zhang, Feng Wang, Xiaofeng Yang, Yikai Wang, Zhongang Cai, Lei Yang, Huaping Liu, and Guosheng Lin. 2024. Gaussianeditor: Swift and controllable 3d editing with gaussian splatting. In *Proceedings of the IEEE/CVF Conference on Computer Vision and Pattern Recognition*. 21476–21485.

[7] Sara Fridovich-Keil, Giacomo Meanti, Frederik Rahbæk Warburg, Benjamin Recht, and Angjoo Kanazawa. 2023. K-planes: Explicit radiance fields in space, time, and appearance. In *Proceedings of the IEEE/CVF Conference on Computer Vision and Pattern Recognition*. 12479–12488.

[8] Michelle Guo, Alireza Fathi, Jiajun Wu, and Thomas Funkhouser. 2020. Object-centric neural scene rendering. *arXiv preprint arXiv:2012.08503* (2020).

[9] Ayaan Haque, Matthew Tancik, Alexei A Efros, Aleksander Holynski, and Angjoo Kanazawa. 2023. Instruct-nerf2nerf: Editing 3d scenes with instructions. In *Proceedings of the IEEE/CVF International Conference on Computer Vision*. 19740–19750.

[10] Amir Hertz, Ron Mokady, Jay Tenenbaum, Kfir Aberman, Yael Pritch, and Daniel Cohen-Or. 2022. Prompt-to-prompt image editing with cross attention control. *arXiv preprint arXiv:2208.01626* (2022).

[11] Jonathan Ho, Ajay Jain, and Pieter Abbeel. 2020. Denoising diffusion probabilistic models. *Advances in neural information processing systems* 33 (2020), 6840–6851.

[12] Edward J Hu, Yelong Shen, Phillip Wallis, Zeyuan Allen-Zhu, Yuanzhi Li, Shewen Wang, Lu Wang, and Weizhu Chen. 2021. Lora: Low-rank adaptation of large language models. *arXiv preprint arXiv:2106.09685* (2021).

[13] Yi-Hua Huang, Yang-Tian Sun, Ziyi Yang, Xiaoyang Lyu, Yan-Pei Cao, and Xiaojuan Qi. 2024. Sc-gs: Sparse-controlled gaussian splatting for editable dynamic scenes. In *Proceedings of the IEEE/CVF Conference on Computer Vision and Pattern Recognition*. 4220–4230.

[14] Bahjat Kawar, Shiran Zada, Oran Lang, Omer Tov, Huiwen Chang, Tali Dekel, Inbar Mosseri, and Michal Irani. 2023. Imagic: Text-based real image editing with diffusion models. In *Proceedings of the IEEE/CVF Conference on Computer Vision and Pattern Recognition*. 6007–6017.

[15] Bernhard Kerbl, Georgios Kopanas, Thomas Leimkühler, and George Drettakis. 2023. 3d gaussian splatting for real-time radiance field rendering. *ACM Transactions on Graphics* 42, 4 (2023), 1–14.

[16] Xinyang Li, Zhangyu Lai, Lining Xu, Yansong Qu, Liujuan Cao, Shengchuan Zhang, Bo Dai, and Rongrong Ji. 2024. Director3D: Real-world Camera Trajectory and 3D Scene Generation from Text. *arXiv preprint arXiv:2406.17601* (2024).

[17] Ruoshi Liu, Rundi Wu, Basile Van Hoorick, Pavel Tokmakov, Sergey Zakharov, and Carl Vondrick. 2023. Zero-1-to-3: Zero-shot one image to 3d object. In *Proceedings of the IEEE/CVF international conference on computer vision*. 9298–9309.

[18] Grace Luo, Trevor Darrell, Oliver Wang, Dan B Goldman, and Aleksander Holynski. 2024. Readout guidance: Learning control from diffusion features. In *Proceedings of the IEEE/CVF Conference on Computer Vision and Pattern Recognition*. 8217–8227.

[19] Ben Mildenhall, Pratul P Srinivasan, Matthew Tancik, Jonathan T Barron, Ravi Ramamoorthi, and Ren Ng. 2021. NeRF: Representing Scenes as Neural Radiance Fields for View Synthesis. *Commun. ACM* 65, 1 (2021), 99–106.

[20] Chong Mou, Xintao Wang, Jiechong Song, Ying Shan, and Jian Zhang. 2023. Dragondiffusion: Enabling drag-style manipulation on diffusion models. *arXiv preprint arXiv:2307.02421* (2023).

[21] Thomas Müller, Alex Evans, Christoph Schied, and Alexander Keller. 2022. Instant neural graphics primitives with a multiresolution hash encoding. *ACM transactions on graphics (TOG)* 41, 4 (2022), 1–15.

[22] Shen Nie, Hanzhong Allan Guo, Cheng Lu, Yuhao Zhou, Chenyu Zheng, and Chongxuan Li. 2023. The blessing of randomness: Sde beats ode in general diffusion-based image editing. *arXiv preprint arXiv:2311.01410* (2023).

[23] Julian Ost, Fahim Mannan, Nils Thuerey, Julian Knott, and Felix Heide. 2021. Neural scene graphs for dynamic scenes. In *Proceedings of the IEEE/CVF Conference on Computer Vision and Pattern Recognition*. 2856–2865.

[24] Xingang Pan, Ayush Tewari, Thomas Leimkühler, Lingjie Liu, Abhimitra Meka, and Christian Theobalt. 2023. Drag your gan: Interactive point-based manipulation on the generative image manifold. In *ACM SIGGRAPH 2023 Conference Proceedings*. 1–11.

[25] Yong-Hyun Park, Minki Kwon, Jaewoong Choi, Junghyo Jo, and Youngjung Uh. 2023. Understanding the Latent Space of Diffusion Models through the Lens of Riemannian Geometry. In *Advances in Neural Information Processing Systems*, A. Oh, T. Naumann, A. Globerson, K. Saenko, M. Hardt, and S. Levine (Eds.), Vol. 36. Curran Associates, Inc., 24129–24142. https://proceedings.neurips.cc/paper_files/paper/2023/file/4bfcebedf7a2967c410b64670f27f904-Paper-Conference.pdf

[26] Ben Poole, Ajay Jain, Jonathan T Barron, and Ben Mildenhall. 2022. Dreamfusion: Text-to-3d using 2d diffusion. *arXiv preprint arXiv:2209.14988* (2022).

[27] Yansong Qu, Shaohui Dai, Xinyang Li, Jianghang Lin, Liujuan Cao, Shengchuan Zhang, and Rongrong Ji. 2024. Goit: Find 3d gaussians of interest with an optimizable open-vocabulary semantic-space hyperplane. In *Proceedings of the 32nd ACM International Conference on Multimedia*. 5328–5337.

[28] Yansong Qu, Yuze Wang, and Yue Qi. 2023. Sg-nerf: Semantic-guided point-based neural radiance fields. In *2023 IEEE International Conference on Multimedia and Expo (ICME)*. IEEE, 570–575.

[29] Aditya Ramesh, Prafulla Dhariwal, Alex Nichol, Casey Chu, and Mark Chen. 2022. Hierarchical text-conditioned image generation with clip latents. *arXiv preprint arXiv:2204.06125* 1, 2 (2022), 3.

[30] Christoph Schuhmann, Romain Beaumont, Richard Vencu, Cade Gordon, Ross Wightman, Mehdi Cherti, Theo Coombes, Aarush Katta, Clayton Mullis, Mitchell Wortsman, et al. 2022. Laion-5b: An open large-scale dataset for training next generation image-text models. *Advances in Neural Information Processing Systems* 35 (2022), 25278–25294.

[31] Yujun Shi, Jun Hao Liew, Hanshu Yan, Vincent YF Tan, and Jiashi Feng. 2024. InstaDrag: Lightning Fast and Accurate Drag-based Image Editing Emerging from Videos. *arXiv preprint arXiv:2405.13722* (2024).

[32] Yujun Shi, Chuhui Xue, Jun Hao Liew, Jiachun Pan, Hanshu Yan, Wenqing Zhang, Vincent YF Tan, and Song Bai. 2024. Dragdiffusion: Harnessing diffusion models for interactive point-based image editing. In *Proceedings of the IEEE/CVF Conference on Computer Vision and Pattern Recognition*. 8839–8849.

[33] Jiaming Song, Chenlin Meng, and Stefano Ermon. 2020. Denoising diffusion implicit models. *arXiv preprint arXiv:2010.02502* (2020).

[34] Junjie Wang, Jiemin Fang, Xiaopeng Zhang, Lingxi Xie, and Qi Tian. 2024. Gaussianeditor: Editing 3d gaussians delicately with text instructions. In *Proceedings of the IEEE/CVF Conference on Computer Vision and Pattern Recognition*. 20902–20911.

[35] Yuze Wang, Junyi Wang, Yansong Qu, and Yue Qi. 2023. Rip-nerf: learning rotation-invariant point-based neural radiance field for fine-grained editing and compositing. In *Proceedings of the 2023 ACM International Conference on Multimedia Retrieval*. 125–134.

[36] Zhengyi Wang, Cheng Lu, Yikai Wang, Fan Bao, Chongxuan Li, Hang Su, and Jun Zhu. 2024. Prolificdreamer: High-fidelity and diverse text-to-3d generation with variational score distillation. *Advances in Neural Information Processing Systems* 36 (2024).

[37] Jing Wu, Jia-Wang Bian, Xinghui Li, Guangrun Wang, Ian Reid, Philip Torr, and Victor Adrian Prisacariu. 2025. Gaussctrl: Multi-view consistent text-driven 3d gaussian splatting editing. In *European Conference on Computer Vision*. Springer, 55–71.

[38] Tianhan Xu and Tatsuya Harada. 2022. Deforming radiance fields with cages. In *European Conference on Computer Vision*. Springer, 159–175.

[39] Bangbang Yang, Chong Bao, Junyi Zeng, Hujun Bao, Yinda Zhang, Zhaopeng Cui, and Guofeng Zhang. 2022. Neumesh: Learning disentangled neural mesh-based implicit field for geometry and texture editing. In *European Conference on Computer Vision*. Springer, 597–614.

[40] Bangbang Yang, Yinda Zhang, Yinghao Xu, Yijin Li, Han Zhou, Hujun Bao, Guofeng Zhang, and Zhaopeng Cui. 2021. Learning object-compositional neural radiance field for editable scene rendering. In *Proceedings of the IEEE/CVF International Conference on Computer Vision*. 13779–13788.

[41] Xiaofeng Yang, Yiwen Chen, Cheng Chen, Chi Zhang, Yi Xu, Xulei Yang, Fayao Liu, and Guosheng Lin. 2023. Learn to optimize denoising scores for 3d generation: A unified and improved diffusion prior on nerf and 3d gaussian splatting. *arXiv preprint arXiv:2312.04820* (2023).

[42] Yu-Jie Yuan, Yang-Tian Sun, Yu-Kun Lai, Yuwen Ma, Rongfei Jia, and Lin Gao. 2022. Nerf-editing: geometry editing of neural radiance fields. In *Proceedings of the*

IEEE/CVF Conference on Computer Vision and Pattern Recognition. 18353–18364.

- [43] Junzhe Zhu, Peiye Zhuang, and Sanmi Koyejo. 2023. Hifa: High-fidelity text-to-3d generation with advanced diffusion guidance. *arXiv preprint arXiv:2305.18766* (2023).
- [44] Jingyu Zhuang, Di Kang, Yan-Pei Cao, Guanbin Li, Liang Lin, and Ying Shan. 2024. Tip-editor: An accurate 3d editor following both text-prompts and image-prompts. *ACM Transactions on Graphics (TOG)* 43, 4 (2024), 1–12.
- [45] Jingyu Zhuang, Chen Wang, Liang Lin, Lingjie Liu, and Guanbin Li. 2023. Dreameditor: Text-driven 3d scene editing with neural fields. In *SIGGRAPH Asia 2023 Conference Papers*. 1–10.
- [46] Zi-Xin Zou, Zhipeng Yu, Yuan-Chen Guo, Yangguang Li, Ding Liang, Yan-Pei Cao, and Song-Hai Zhang. 2024. Triplane meets gaussian splatting: Fast and generalizable single-view 3d reconstruction with transformers. In *Proceedings of the IEEE/CVF Conference on Computer Vision and Pattern Recognition*. 10324–10335.

A IMPLEMENT DETAILS

A.1 Training Setup

For 3DGS reconstruction, we optimized the Gaussians over 7,000 iterations and set the spherical harmonics to degree 0. In our experiment, batch size is set to 4, and the learning rates for Gaussian's color, opacity, scale, and rotation are set to 2.5×10^{-3} , 2.5×10^{-3} , 2.5×10^{-4} , and 2.5×10^{-3} , respectively. The shifts in Gaussian position are entirely obtained through the MTP encoder and the RSP decoder, and we set the learning rate for the MTP encoder was set to 1×10^{-3} , while the learning rate for RSP was 5×10^{-4} . In the first stage, we freeze the Gaussian attributes and only train MTP and RSP. In the second stage, we lower the learning rate of MTP to 1×10^{-4} to stabilize the scene's geometric structure and begin training the other Gaussian attributes. For Drag-SDS, we set $\lambda_{\text{lat}} = 1$, $\lambda_{\text{img}} = 0.1$, and $\lambda_{\text{lora}} = 1$, the learning rate of the learnable embedding \hat{y}_θ set to 1×10^{-3} , and the lora rank set to 16 with the learning rate of 5×10^{-4} .

A.2 Two-Stage Dragging

During the entire training process, we sample the diffusion timestep t using a cosine annealing schedule $t = f(s) = \frac{1}{2}(T_{\text{max}} - T_{\text{min}})(1 + \cos(\pi s)) + T_{\text{min}}$, where s is the current training epoch ratio, $[T_{\text{max}}, T_{\text{min}}] = [0.98, 0.02]$ represents the annealing range for the diffusion timestep. Inspired by previous works that utilized diffusion models based on latent variables for image editing [25, 32], we hypothesize that the diffusion model optimize the overall geometric structure of the image at higher diffusion timesteps ($> 0.7T$), and refining the texture at lower timesteps ($< 0.7T$). Therefore, we derive the two-stage training epochs based on the diffusion timestep, where the chosen timestep threshold is $T_{\text{threshold}} = 0.7$, leading to a first-stage geometric reconstruction training epoch ratio of $s = f^{-1}(T_{\text{threshold}}) = 0.36$

A.3 Classifier-Free Guidance

Here, we provide a detailed description of the classifier-free guidance (CFG) scale we used. Unlike the conventional LDM, which uses a fixed CFG, we follow the approach in [31] and use CFG annealing to avoid the over-saturation issue. Specifically, we employ a CFG inverse square annealing function:

$$\omega(s) = (\omega_{\text{max}} - 1) \times (1 - s)^2 + 1, \text{ with } \omega_{\text{max}} = 4 \quad (12)$$

Our target noise prediction uses CFG, while the source noise prediction does not:

$$\epsilon_{\text{tgt}} = \omega(s)(\epsilon_\theta(z_t, t, y) - \epsilon_\theta(z_t, t, \emptyset)) + \epsilon_\theta(z_t, t, \emptyset) \quad (13)$$

$$\epsilon_{\text{src}} = \hat{\epsilon}_\phi(x_t, t, \hat{y}_\theta) \quad (14)$$

A.4 Total Loss

We optimize the total loss for the 3D Gaussian as follows, where $\lambda_{\text{d-sds}} = 1$, $\lambda_{\text{rr}} = 2500$:

$$\mathcal{L} = \lambda_{\text{drag-sds}} \mathcal{L}_{\text{Drag-SDS}} + \lambda_{\text{rr}} \mathcal{L}_{\text{RR}} \quad (15)$$

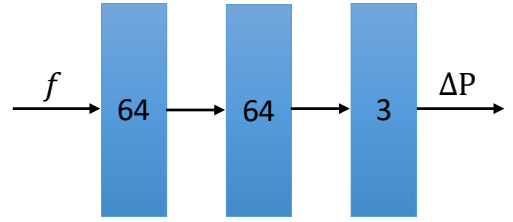


Figure 13: The MLP structure employed in the RSP Decoder.

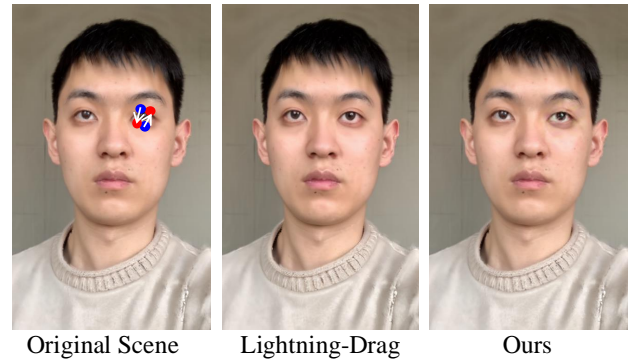


Figure 14: Visualization of our failure case. We render the Gaussian in the corresponding viewpoint to obtain the rendered image and 2D mask, and project the 3D handle points and target points into 2D as the input for Lightning-Drag, the figure illustrates the output results. Lightning-Drag fails in this case, and since our method uses Lightning-Drag as guidance, it also struggles to achieve the desired results.

B DETAILS OF THE RSP DECODER

Fig. 13 present the structure of the MLP employed in our RSP. The MLP accepts multi-scale features f as input and outputs positional shifts ΔP . In our RSP Decoder, there are two such MLPs, \mathcal{N}_1 and \mathcal{N}_2 , which are used to predict positional shifts of Gaussians in the desired and undesired editing area, respectively. In our experiments, we found that directly using \mathcal{N}_2 to predict positional shifts in undesired editing area leads to severe geometric tearing issues. To address this, we designed Eq. (16) to prevent such problems.

$$\Delta p = \begin{cases} \mathcal{N}_1(f), & \text{for } g_i \in \mathcal{G}_m, \\ \text{sg}(\mathcal{N}_1(f)) + \mathcal{N}_2(\text{sg}(f)), & \text{for } g_i \in \mathcal{G}_{\text{um}}, \end{cases} \quad (16)$$

C FAILURE CASE

Since we used the pretrained drag-based LDM Lightning-Drag [31], our method also inherits its failure cases. The Fig. 14 shows the user input where the user expects his eye to be closed, and both Lightning-Drag and our method fail in this case.